OPTIMIZATION OF THE ADDITIVE MANUFACTURING PROCESS FOR GEOMETRICALLY COMPLEX VIBRO-ACOUSTIC METAMATERIALS

T.M. Mukhametkaliyev[1], M. Ferrucci[1, 2], M. Pavan[1], M. C. Villanueva[2,3], T. Craeghs[1], C. Claeys[2,3], E. Deckers[2,3], W. Desmet[2,3]

[1]Materialise NV, Technologielaan 15, 3001 Leuven, Belgium
[2]KU Leuven, Mechanical Engineering Department, Celestijnenlaan 300, 3001 Leuven, Belgium
[3]DMMS lab, Flanders Make

Abstract

A study performed at KU Leuven provided a proof-of-concept of vibro-acoustic locally resonant meta-materials manufactured with Laser Sintering (LS). However, the geometry and material properties of the manufactured parts deviated from their nominal (specified) values, resulting in differences in resonant frequencies of the locally added resonators and a deviation from their predicted vibro-acoustic performance. In this work, the fabrication of locally resonant vibro-acoustic metamaterials was improved through a holistic engineering approach, resulting in an improved vibro-acoustic performance. It is shown that unequal energy density distribution within the printing layers is one of the main causes of deviations.

Keywords: Additive Manufacturing, Laser Sintering, Vibro-acoustic Metamaterial, ED mapping, Up-skin and Down-skin scanning strategy, Scan Pattern, Computer Tomography, Optimization

1. Introduction

The reduction of noise is an important challenge in ensuring healthy living and working environments [1].

As such, there is a demand for the development of compact, lightweight, reliable, and affordable acoustic insulation materials. Vibro-acoustic metamaterials have a high potential, for instance as an acoustic insulator for noise in a targeted, tunable frequency band, referred to as stop band [2-4]. A study performed at KU Leuven serves as a proof-of-concept for meta-materials manufactured with Laser sintering (LS) [4], In this work, an enclosure consisting of arrays of structural resonators was designed (Figure 1). Each resonator consists of two thin legs acting as leaf springs to connect a mass to a host structure, such that a spring-mass-like resonant system is obtained. The inclusion of resonators to the cavities of a sandwich structure leads to pronounced vibration attenuation. This reduced vibrational response, in turn, prevents acoustic transmission from the inside of the enclosure to the outside of the enclosure, and therefore create increased acoustic performance, at least in targeted frequency bands.

The LS manufactured resonators exhibited geometrical and material deviations from their nominal values, which consequently resulted in a discrepancy between the actual and intended resonant frequencies of the added resonators, also altering the predicted resonance frequency, and hence also the vibrational and acoustic behaviour of the enclosure. The dimensions of the manufactured parts were consistently smaller than nominal. Figure 2a shows an example of shape

deviations for the connecting leg where it can also be noticed that the leg is not straight. The nominal and actual (measured) dimensions are shown in Figure 2b; the largest errors were observed for the thickness of the connecting leg and the resonator mass. Both of these features strongly affect the resonance frequency of the structure. The thickness of the connecting legs dictates the structure's stiffness while the thickness of the mass mainly determines the total vibrating mass of the resonator. Together they affect the vibro-acoustic performance. For example, a deviation in leg thickness of -0.17 mm and a deviation in resonator mass thickness of -0.15 mm resulted in a deviation in stop band frequencies from the intended 1065 - 1226 Hz to 600 - 661 Hz [4]. Moreover it was reported that the actual weight of enclosure was significantly lower than predicted, which might indicate a lower quality of sintering and thus a higher porosity [4].

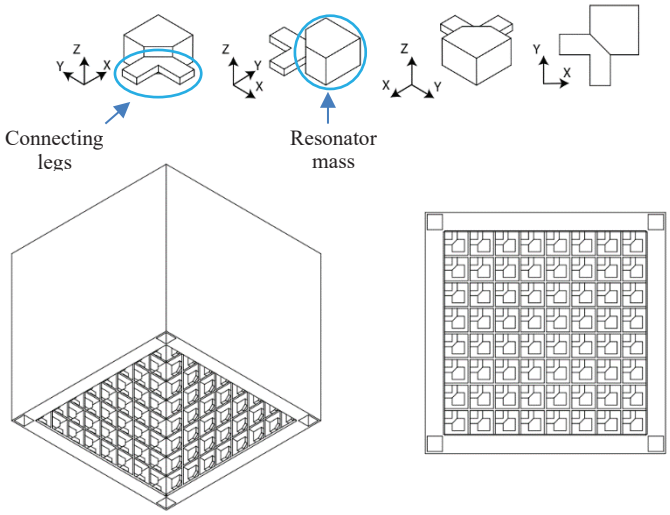

Figure 1. Structural resonator (top) and enclosure design (bottom) [4].

There is therefore a need to improve the LS manufacturing of vibro-acoustic metamaterials to ensure that the parts achieve their intended vibro-acoustic performance.

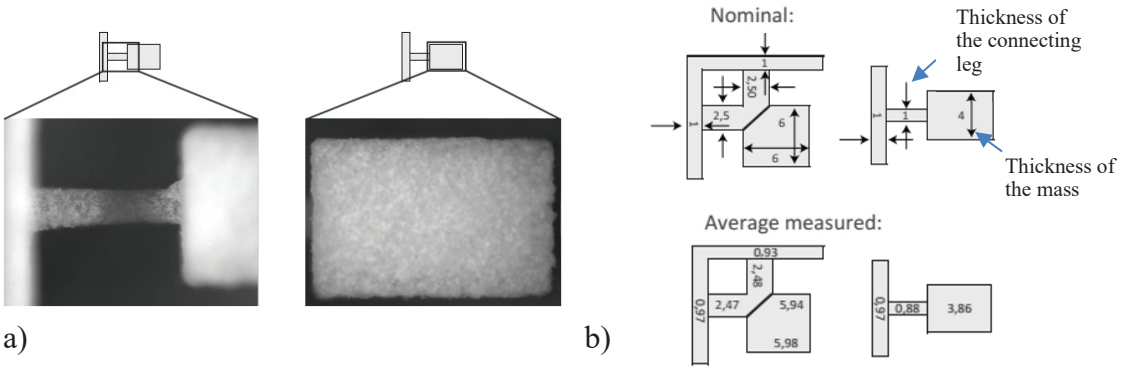

Figure 2. a) On the left we show one of the connecting legs, which was not straight, and on the right side we show a resonator mass. b) Characteristic dimensions from a strip of resonator cells. On the top the dimensions as defined in the CAD file are shown. The average measured distances for each resonator are depicted on the bottom. [4]

LS has the ability to produce freeform complex structures, which are not manufacturable by traditional manufacturing technologies [5-7]. Parts with complex geometries, such as the structural resonators, typically contain features of various shapes and sizes that are difficult to manufacture within the required tolerances. In fact, both the slicing process, which discretizes the part into process-layers, and the local processing conditions determined by feature's size and scanning strategy, have an influence on the local dimensions [8]. Manufactured dimensions are also affected by non-uniform energy density (ED) during production. Modelling the energy density prior to a build, particularly for areas near the part edge, can be useful in ensuring a more homogeneous deposition of energy for complex geometries [9].

Non-uniform thermal history during production also affects part properties [10]. Heat dissipation depends on whether the layers below or above are sintered (Figure 3). The finite depth of the melt pool means that lower layers are re-melted multiple times. Recrystallization therefore occurs with a time delay and at a particular depth (usually a few centimeters) below subsequently sintered layers [11] . For inner volume (in-skin) layers, this re-melting occurs relatively uniformly. There might be an exception, however, in the case of upward facing (up-skin) layers. Subsequent layers are not melted, which means that re-melting of upper layers (up to and including the last sintered layer) is not consistent with the re-melting of in-skin layers. As a result, materials in regions near up-skin layers are not completely sintered and might exhibit higher porosity. Furthermore, powders below down-skin layers might be partially melted by the significant heat deposited on the down-skin layer. This effect contributes to dimensional deviations for downward facing surfaces. These effects might be exacerbated in the production of parts with complex shapes and small features, such as those found in structural resonators of vibro-acoustic metamaterials, which exhibit decreased resonant frequencies in the presence of such discontinuities. To the knowledge of the authors, the influence of modifying the deposited energy for up-skin and down-skin layers on the acoustic performance of structural resonators has not been studied in the literature. The amount of deposited energy and the slicing process should be adapted to ensure proper sintering for up-skin and down-skin layers. In this study, the effect of adapting scanning speed for up-skin and down-skin layers on the LS production of structural resonators is investigated.

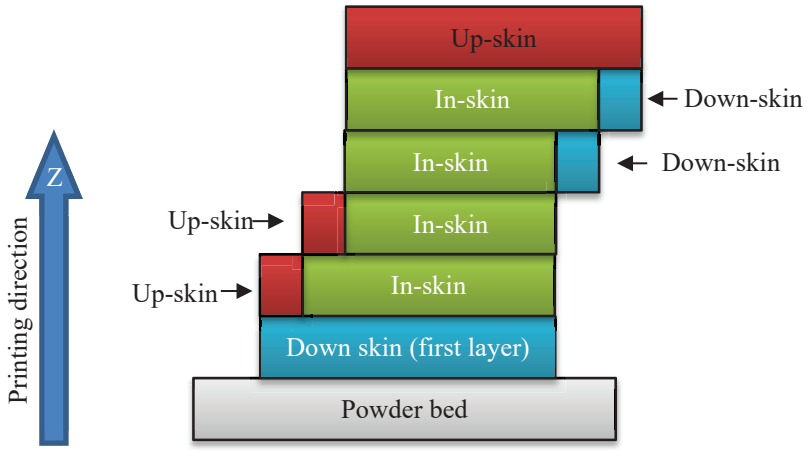

Figure 3. Schematic view of up-skin and down-skin layers.

2. Methods and experimental procedure.

A schematic workflow for the optimization of the manufactured vibroacoustic metamaterials is shown in Figure 4. Analysis of the part's actual properties can be used in a feedback for optimizing the manufacturing parameters to achieve the targeted properties. In this study, it is sought to reduce the difference between the actual and targeted vibrational properties of structural resonators by adapting the LS parameters. Local energy density mapping is used to determine non-uniformities in energy deposition, while X-ray computed tomography (CT) is used to measure the dimensions and porosity of manufactured parts.

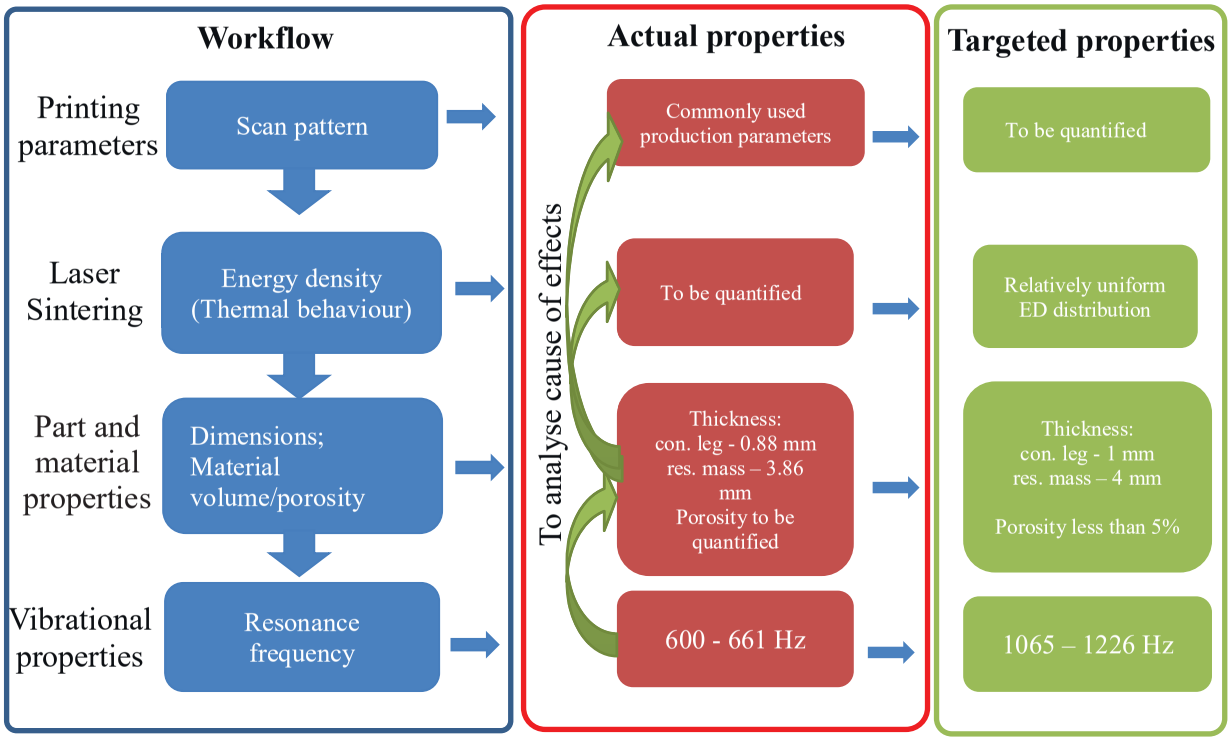

Figure 4. Workflow of production process optimization, interinfluence of the workflow blocks, actual and targeted performance of vibro-acoustic metamaterials

2.1. Samples production

The vibro-acoustic resonator samples are produced in a state-of-the-art laser sintering machine, equipped with the new Materialise Control Platform (MCP) [12] using a PA2200 PA12 powder with a virgin/recycled mixing ratio of 50/50 and a layer thickness of 120 microns.

2.2 Energy Density mapping

Local energy density (ED) mapping models the deposition of energy in LS production given the laser parameters, scanning strategy, part geometry, and part orientation in the build. By creating an ED map, it is possible to pre-assess the uniformity of the deposited energy and identify regions of excessive energy, which can result in dimensional deviations, or regions of inadequate energy,

which result in the generation of pores [9]. The ED maps used in this work have a pixel size of 12.8 µm. The defined region of optimal sintering window was calculated using the equation describing the surface ED formulation [13]:

$$ED = \frac{LP}{SS\ x\ HD}, \quad (1)$$

where LP is the Laser Power, SS the Scanning Speed and HD is the Hatching Distance.

Figure 5 shows the ED range which allows to obtain optimal porosity/density, mechanical properties and dimensional accuracy.

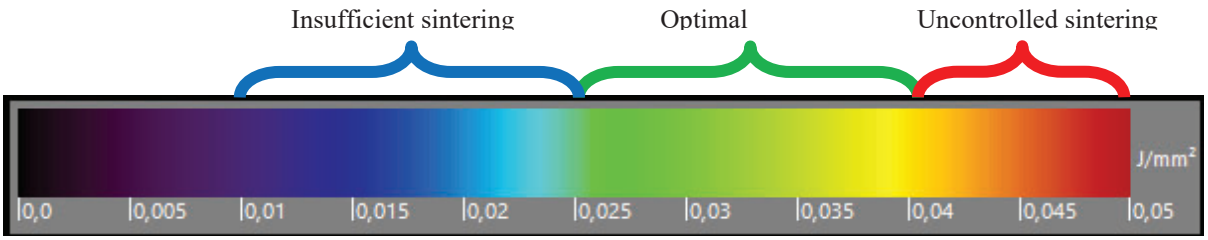

Figure 5. Optimal ED sintering window

It is also possible to define an ED range yielding insufficient sintering and one for high ED values which lead to uncontrolled sintering (i.e. dimensional deviations).

2.3 CT.

CT is a non-destructive technique that allows the measurement of internal and external structures as well as porosity of a part [8].

CT measurements were performed using a Nikon XT H 225 ST (Nikon Metrology) using a Molybdenum X-ray source target, an electron acceleration voltage of 110 kV, and a filament current of 127 µA. A magnification factor of 11 was used, yielding a voxel size of 18 µm. A set of 3142 X-ray projection images were acquired of the samples and subsequently reconstructed into a voxel volume by filtered back projection in CT Pro 3D software (Nikon Metrology). The CT reconstructed volumes are analysed using VGStudio MAX 3.2 (Volume Graphics GmbH).

2.4 Vibrational measurements

Ideally, the acoustic performance of the entire enclosure is evaluated. Since this would require printing each time an entire enclosure, in this paper it is chosen to evaluate the vibrational properties, i.e. the resonance frequency, of the structural resonators. This choice is justified since the acoustic properties of the acoustic enclosure in the stop band frequency region directly results from the resonance frequency of the structural resonators. In order to evaluate the vibrational performance from the samples, two main characteristics are measured: resonance frequency and the damping of each resonator. The resonance frequency is determined by attaching each printed sample to a rigid metal base which is connected to a shaker (Figure 6). Each sample was attached to the base using double-sided tape, thereby not affecting the material properties of the printed

samples. The vibration response of the resonator is measured at the mass-part of the resonator using a Scanning Polytec PSV-500 Laser Doppler Vibrometer (LDV) [14].

The resonance frequency is acquired as the frequency where the peak of the measured frequency response function occurs. Measurement repeatability was determined by repeating each measurement 3 times at 30-minute intervals. The modal damping is obtained applying the half-power bandwidth method [15].

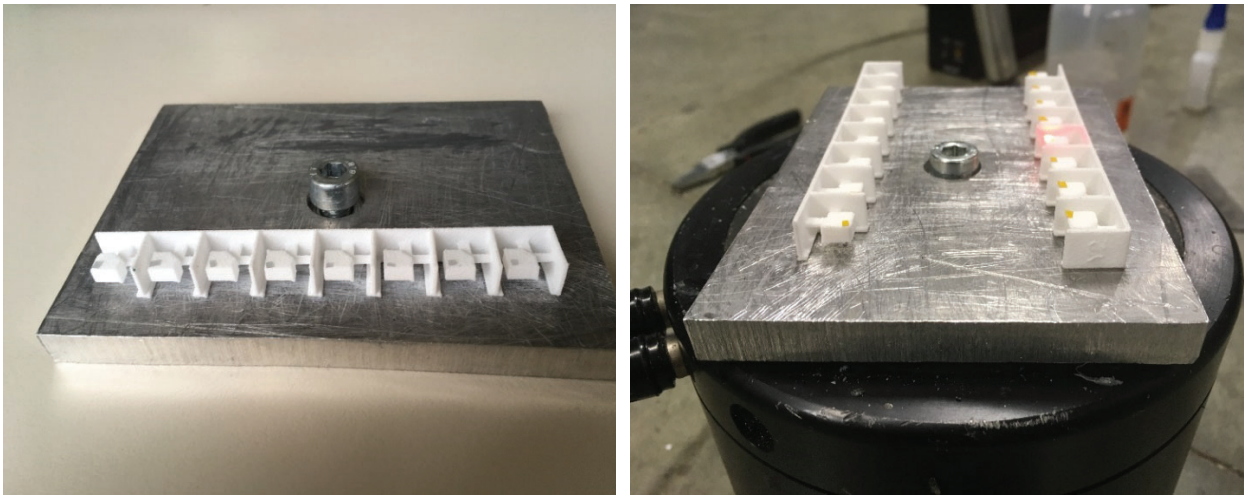

Figure 6. Vibrational measurements of resonators with Scanning Polytec PSV-500 Laser Doppler Vibrometer.

2.5 Design of Experiments

The builds of the samples of structural resonators have been prepared using Magics v22.1 (Materialise NV) [16] and sliced using the StandardSLx Build Processor (BP) v2.3 (Materialise NV) [12]. Analysis on up/down-skin contour borders distribution was performed using Materialise Inspector 3.2.0.2003 (Materialise NV) [17].

In a previous study [1], the acoustic enclosure was produced such that each edge was oriented at 45 degrees with respect to the Cartesian axes of the build platform (Figure 7, a). All resonator structures were therefore manufactured in similar build orientations to avoid variations in the vibro-acoustic performance within the enclosure. In this study, strips of 8 resonators were produced along three axes (hence referred to as X, Y, and Z axes) each oriented at 45 degrees with respect to the build platform (Figure 7, b). These axes were chosen to correspond to the edges of the enclosure built in [1]. For each axis, three strips were produced and labeled numerically, i.e. X1, X2, X3, Y1, Y2, Y3, Z1, Z2 and Z3.

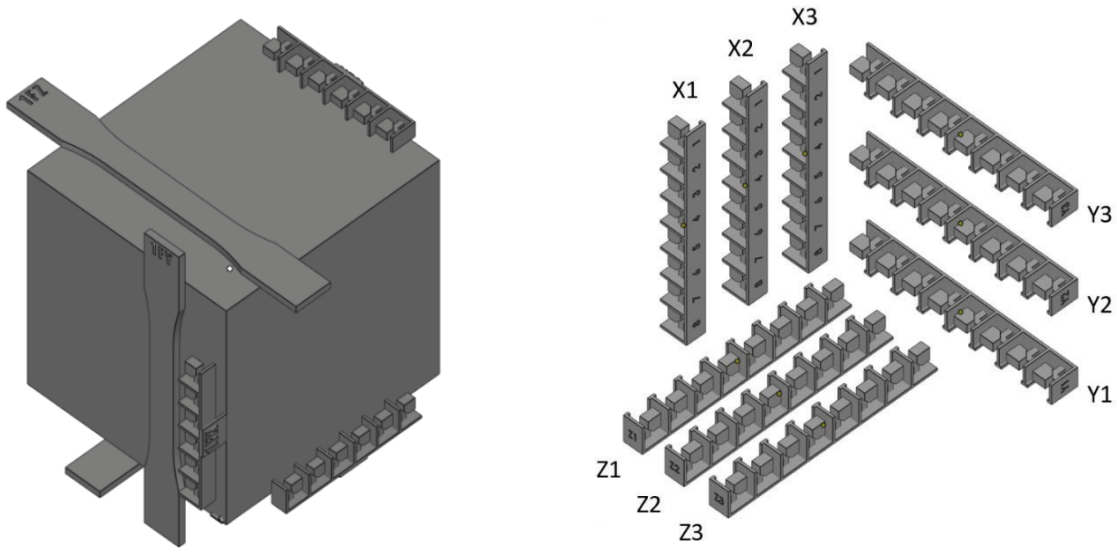

a) b)

Figure 7. Orientation of acoustic enclosure and design of samples

Typically, the laser hatching direction is alternated by 90° between adjacent layers, henceforth referred to as 0/90°. In this study, for the first scanning strategy alternated the hatching direction in a 5/125/245° strategy, that is in increments of 120°. This strategy has been selected, since it was found that the generated scan pattern improves the homogeneity of the energy delivered at the edge of the resonators, and may influence the local dimensions [18]. This scanning strategy will be referred further in the study as 'optimized scan pattern strategy'.

Also the effect of adapting scanning speed for up-skin and down-skin layers to compensate for insufficient and excess deposited energies, respectively was studied. These adaptations are made on the optimized scan pattern strategy. Up-skin and down-skin layers are identified in BP as those layers that are inclined by 50° or less with respect to the horizontal build plane (Figure 8). Up-skin and down-skin regions are deposited as contours, i.e. no scan hatching was implemented for these regions. To compensate for insufficient energy in up-skin areas, a scanning speed of 2500 mm/s was applied for corresponding contour vectors in 'up/down-skin strategy 1'. Based on feedback from the parts build with 'up/down-skin strategy 1', a scanning speed of 2000 mm/s was applied for 'up/down-skin strategy 2'. To compensate for excess energy in down-skin areas, a scanning speed of 3500 mm/s was applied in both 'up/down-skin strategy 1' and 'up/down-skin strategy 2'. In this study it is not possible to generate ED maps for the up/down-skin strategies since it requires additional calculation in the simulation program. Therefore, values of optimized scanning speed for up/down-skin contour vectors were chosen as equivalent deviations above and below the reference scanning speed.

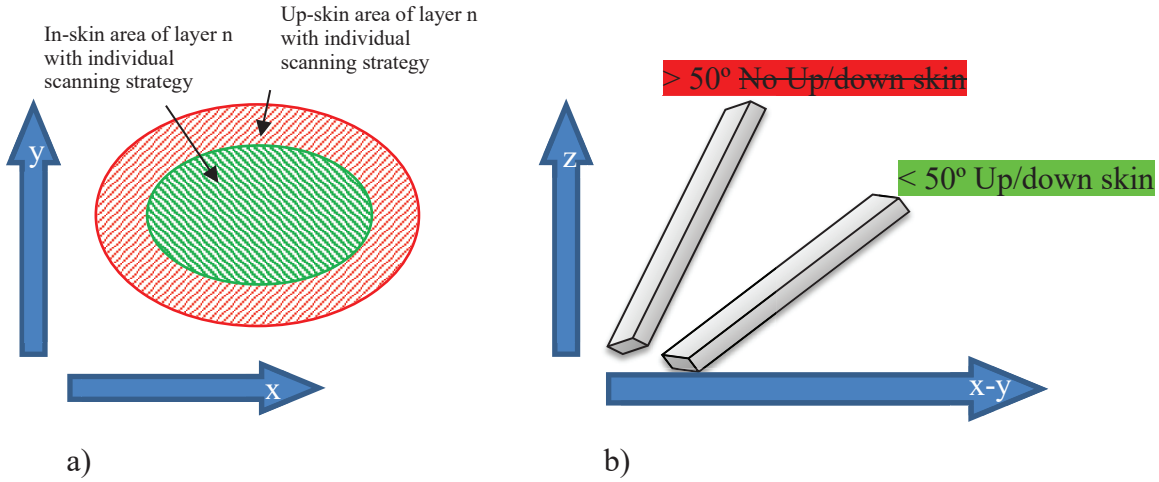

Figure 8. Schematic view of dedicated scanning strategy for up skin and down skin layers.

The laser scanning parameters used to manufacture the samples in this study are summarized in Table 1. The reference strategy in Table 1 shows the common process parameters used in manufacturing of LS polyamide parts.

Table 1. LS process parameters used to produce samples.

Scanning strategy		Contour Laser Power (W)	Contour Scanning Speed (mm/s)	Hatching Laser Power (W)	Hatching Scanning Speed (mm/s)	Hatching Scan Spacing (mm)	Inclination of scan pattern (º)
Reference		34	3000	40	4000	0.3	0/90
Optimized scan pattern strategy		34	3000	40	4000	0.3	5/125/245
Up/down-skin strategy 1	In skin	34	3000	40	4000	0.3	5/125/245
	Up skin 1		2500				
	Down skin 1		3500				
Up/down-skin strategy 2	In skin		3000		4000		5/125/245
	Up skin 2		2000				
	Down skin 2		3500				

3. Results and discussion

3.1 Optimized scan pattern.

In Figure 9a a cross-sectional cutaway resonator from one of the Y oriented strips. The ED map for the resonator built using the reference scanning strategy is shown in Figure 9b and exhibits zones of excessive and inadequate deposited energy. The ED map for the resonator built using the 'optimized scan pattern' strategy is shown in Figure 9c and exhibits a more uniform distribution of energy. The high energy zone in Figure 9b is a result of significant overlapping between adjacent

laser paths; the laser beam diameter in this study is 0.6 mm. Despite the improvement in the energy distribution within the main region of the part, high energy regions near corners remained despite the adapted scanning strategy. CT cross-sectional images of the samples printed with reference and 'optimized scan pattern' strategies are shown in Figure 9b and Figure 9c, respectively. The solid lines in these figures correspond to the nominal triangulated surface, which was best-fit aligned to the surface thresholded CT datasets. The dimensions of the samples printed with the 'optimized scan pattern' strategy are visually closer to the nominal dimensions of the triangulated surfaces. In Table 2 the measured thicknesses of the connecting leg and resonator mass, measured porosity percentage, and the measured resonant frequencies for samples built with the reference and 'optimized scan pattern' strategies is shown. The deviation of the leg and resonator mass thicknesses from nominal was reduced in the 'optimized scan pattern' samples. Also, variation in these thicknesses along all printed resonator structures decreased in the 'optimized scan pattern' samples. The porosity percentage in the reference samples was 15.44 %, while porosity percentage in the 'optimized scan pattern' samples was 8.22 %.

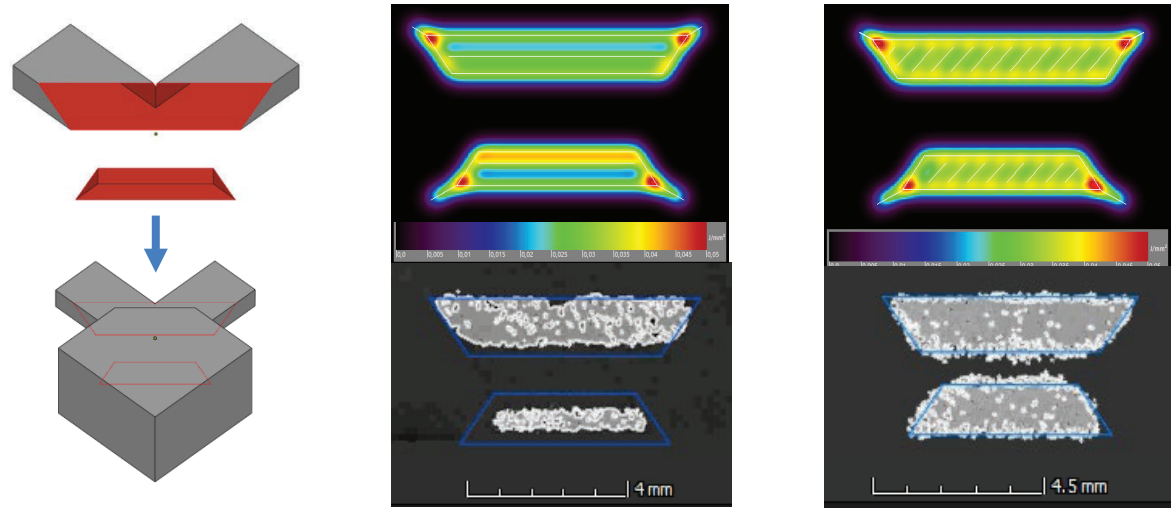

a) b) c)

Figure 9. Comparison of ED maps before and after optimization for Y-strip resonator. a) Cross-sectional cutaway of a resonator. b) ED map and corresponding CT slice of reference sample. c) ED map and corresponding CT slice of 'optimized scan pattern'. The solid lines at the bottom of (b) and (c) are the contours of the nominal model after best-fit alignment to the surface-thresholded CT volumes.

The improvement in the manufactured dimensions of the 'optimized scan pattern' samples is reflected in their higher resonant frequencies. Resonance frequency results are consistent between the strips within one orientation for a given scanning strategy. The largest variation in measured resonance frequencies occurs for the samples printed in the Y-direction. As a result of decreased porosity, the average measured volume of sintered material for a single resonator increased from 112.80 mm^3 in the reference scan pattern to 133.59 mm^3 in the optimized scan pattern.

3.2 Up-skin / down-skin strategy 1 and 2.

Samples produced with the up-skin/down-skin strategies exhibited further improvements in resonant frequencies and porosity percentage in comparison with 'optimized scan pattern' (Table 2).

Table 2. Average measured thickness of connection legs and resonator mass, average volume and porosity, and vibroacoustic measurements of a single resonator.

	Orientation	Thickness of connecting leg		Thickness of mass		Average volume of single resonator [mm^3]	Average porosity [%]	Resonance frequency	
		Average [mm]	Std. dev.	Average [mm]	Std. dev.			Average [Hz]	Std. dev.
Reference	**X**	0.79	0.027	3.76	0.013	112.8	15.44	628.58	30.1
	Y	0.81	0.017	3.78	0.004			660.88	18.35
	Z	0.77	0.006	3.75	0.006			599.83	11.46
Optimized scan pattern	**X**	1.03	0.042	3.97	0.021	133.59	8.21	826.39	30.35
	Y	1.00	0.037	3.92	0.061			798.02	42.43
	Z	1.05	0.025	4.00	0.028			835.98	30.1
Up/down-skin strategy 1	**X**	1.09	0.017	4.02	0.007	157.21	2.75	1174.62	26.78
	Y	0.99	0.026	3.97	0.012			999.76	14.06
	Z	1.08	0.008	4.02	0.004			1172.39	33.33
Up/down-skin strategy 2	**X**	1.09	0.018	4.03	0.009	155.46	3.02	1198.44	12.87
	Y	1.06	0.016	4.04	0.007			1130.94	6.69
	Z	1.08	0.019	4.04	0.003			1183.69	10.43

Similarly to the results observed in the optimized scan pattern, Y-strip samples exhibited lower resonance frequencies than samples in the X and Z-strips. We therefore analyzed the total lengths of up-skin and down-skin surfaces for each strip orientation using Materialise Inspector. Samples in the Y-strip had in total almost two times higher length of the contour borders belonging to up/down-skin areas in comparison with samples in X and Z-directions (Table 3). This result could suggest that Y oriented resonators are more susceptible to insufficient or excessive energy supply for up-skin and down-skin layers, respectively. CT slices in Figure 8 demonstrate that for 'up/down-skin strategy 1' there is an improvement in the dimensional accuracy of the built samples when compared to the optimized scan pattern. However, a rough edge of up/skin contour layer for 'up/downskin strategy 1' was observed for most of the contour slices. As shown in Figure 8 and by the results summarized in Table 2, these inconsistencies were significantly reduced in the samples with the up/down-skin strategy 2.Furthermore, variations in results among samples build in the same orientation were also reduced in the up/down-skin strategy 2.

Table 3. Analysis of contour types of borders distribution for up/down-skin strategies

Orientation along principal axe		X	Y	Z
Lenght of of border [mm]	Up-skin	146,55	347,2	191,03
	Down-skin	217,87	455,97	172,73
	Normal	989,35	502,15	989,9329
	Total	1353,77	1305,32	1353,6915

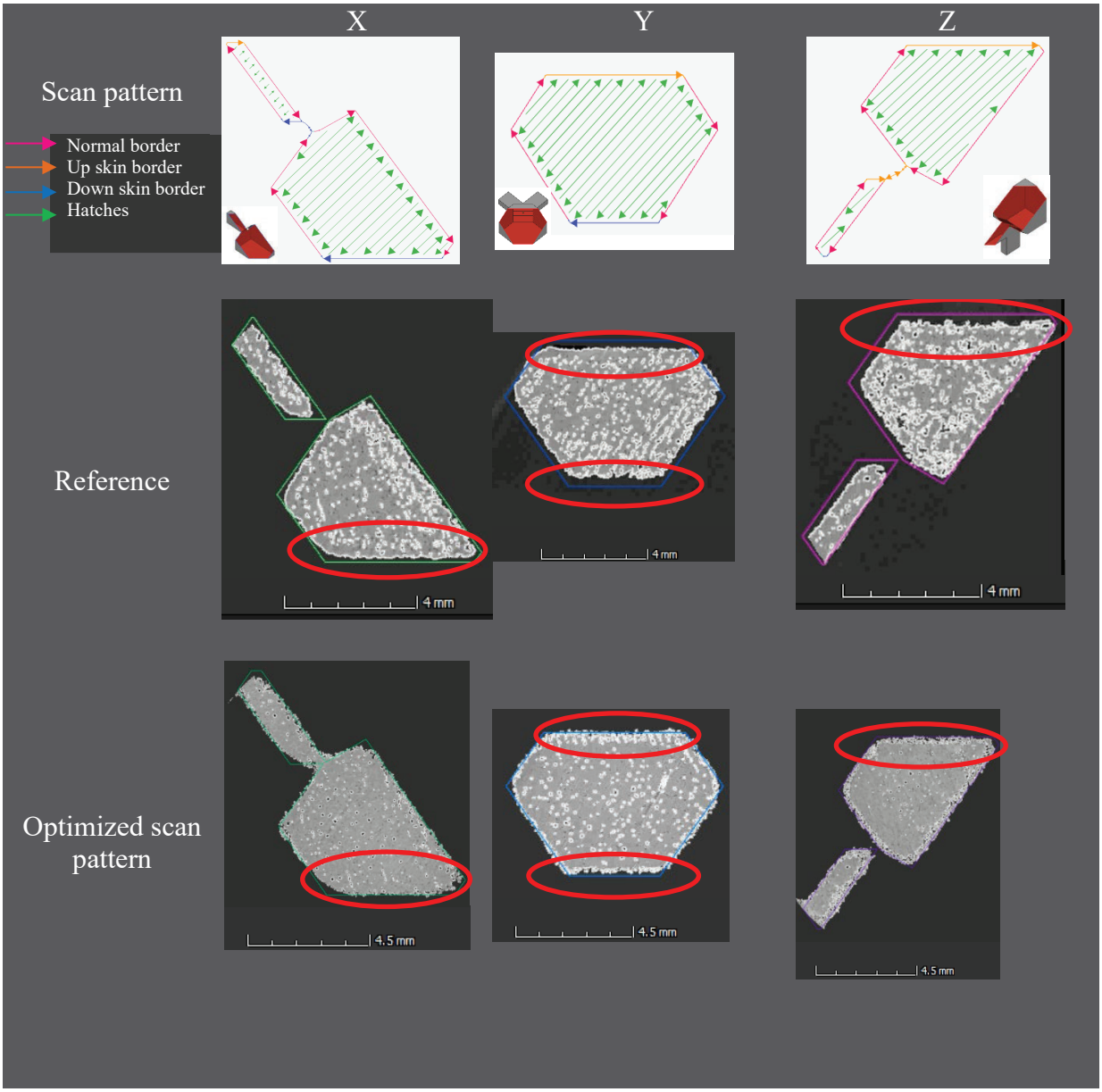

Figure 10 continues on the next page
Continue of Figure 10

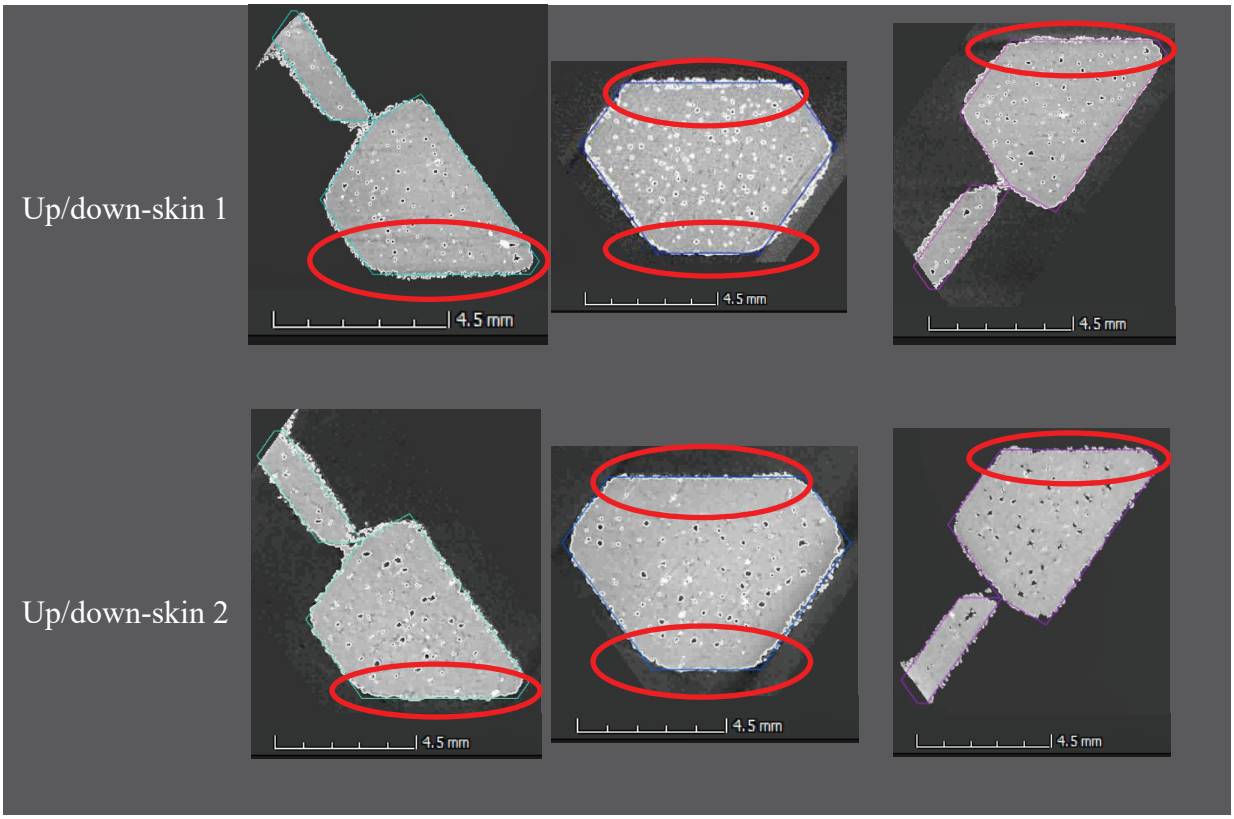

Figure 10. Comparison of scan pattern with CT slice for all scanning strategies. Samples of X, Y, Z-directions are best-fit aligned to the surface thresholded CT datasets.

From Figure 10. and summarized results of Table 2 it is seen that 'up/down-skin strategy 2' achieved the targeted properties through application of dedicated energy input for up skin and down-skin layers. A higher consistency along resonators of X, Y, Z directions are observed.

4. Conclusion

In this study the effect of adapting the scanning strategy, namely the angle with which the hatching direction is alternated for adjacent layers, in the LS manufacture of vibro-acoustic metamaterials is investigated. Geometrical (dimensional) and material (porosity) deviations from nominal were reduced when using a 'optimized scanning strategy'. The thickness of the connection legs and resonator mass were strongly affected by poor sintering of powder near contour vectors. X-ray computed tomography was used to evaluate the dimensions and porosity of the built parts. The vibrational performance of the samples built using an 'optimized scanning strategy' improved when compared to the same performance using a common production strategy (reference).

The targeted vibrational properties were achieved when implementing 'up/skin down-skin strategy 1' and 'up/skin down-skin strategy 2'. Insufficient energy deposition for up-skin layers resulted in increased porosity and dimensional deviations. By adapting the scanning speed for up-skin and down-skin layers, porosity and dimensional deviations in up/down-skin layers were reduced, and therefore the performance of laser sintered acoustic metamaterials was improved.

The results of this study serve to inform further optimization of the LS manufacture of acoustic metamaterials and other small and complex parts.

Acknowledgements

The authors would like to acknowledge the KU Leuven Research Fund and the Materialise R&D for its support. This research is also partially supported by Flanders Make, the strategic Research Centre for the Manufacturing Industry. The research of M. Clasing Villanueva is funded by a PhD CONICyT Becas Chile scholarship. Elke Deckers is a postdoctoral fellow of the Research Foundation – Flanders (F.W.O). This work has also received funding from the European Union the frame of the MSCA ACOUTECT project under grant agreement No. 721536.

References

[1] WHO, Burden of disease from environmental noise, The Regional Office for Europe of the World Health Organization (Bohn) (2011).
[2] S.A. Cummer, J. Christensen, A. Alù, Controlling sound with acoustic metamaterials, Nature Reviews Materials 1 (2016) 16001.
[3] G. Ma, P. Sheng, Acoustic metamaterials: From local resonances to broad horizons, Science Advances 2(2) (2016) e1501595.
[4] C. Claeys, Design and Analysis of Resonant Metamaterials for Acoustic Insulation(Ontwerp en analyse van resonante metamaterialen voor geluidsisolatie), Design and Analysis of Resonant Metamaterials for Acoustic Insulation (2014).
[5] Rapid Manufacturing: An Industrial Revolution for the Digital Age, Rapid Manufacturing, pp. 1-285.
[6] D. Bourell, J.P. Kruth, M. Leu, G. Levy, D. Rosen, A.M. Beese, A. Clare, Materials for additive manufacturing, CIRP Annals 66(2) (2017) 659-681.
[7] R.D. Goodridge, C.J. Tuck, R.J.M. Hague, Laser sintering of polyamides and other polymers, Progress in Materials Science 57(2) (2012) 229-267.
[8] M. Pavan, T. Craeghs, R. Verhelst, O. Ducatteeuw, J.-P. Kruth, W. Dewulf, CT-based quality control of Laser Sintering of Polymers, Case Studies in Nondestructive Testing and Evaluation 6 (2016) 62-68.
[9] M. Pavan, P. Van Den Ecker, T. Craeghs, J.-P. Kruth, W. Dewulf, Investigating the influence of the energy density distribution on the quality of laser sintered polyamide-12 parts by using X-Ray Computed Tomography, 2017.
[10] H. Zarringhalam, N. Hopkinson, N.F. Kamperman, J.J. de Vlieger, Effects of processing on microstructure and properties of SLS Nylon 12, Materials Science and Engineering: A 435-436 (2006) 172-180.
[11] A. Wegner, G. Witt, Understanding the decisive thermal processes in laser sintering of polyamide 12, AIP Conference Proceedings 1664(1) (2015) 160004.

[12] https://www.materialise.com/en/software/control-platform.
[13] D. Bourell, J. Coholich, A. Chalancon, A. Bhat, Evaluation of energy density measures and validation for powder bed fusion of polyamide, CIRP Annals 66(1) (2017) 217-220.
[14] P.G.P.-S.V.D.h.w.p.c.u.v.p.f.-f. ld-vibrometers/psv-500-scanning-vibrometer/.
[15] B.A. Olmos, J.M. Roesset, Evaluation of the half-power bandwidth method to estimate damping in systems without real modes, Earthquake Engineering & Structural Dynamics 39(14) (2010) 1671-1686.
[16] https://www.materialise.com/en/software/magics.
[17] https://www.materialise.com/en/software/inspector.
[18] M. Pavan, M. Sinnaeve, S. Leyssens, T. Craeghs, J.-P. Kruth, W. Dewulf, Determining the dimensional accuracy limits of laser sintered PA12-parts: from artefact design to dimensional characterization by X-Ray Computed Tomography, 2017.